Investigation of the Radial Deformability of Individual Carbon Nanotubes under Controlled Indentation Force

Min-Feng Yu,[1] Tomasz Kowalewski,[2,*] and Rodney S. Ruoff[1,†]

[1]*Department of Physics, Washington University in St. Louis, St. Louis, Missouri 63130*

[2]*Department of Chemistry, Washington University in St. Louis, St. Louis, Missouri 63130*

(Received 30 March 2000)

Tapping-mode atomic force microscopy was used to study the radial deformability of a multiwalled carbon nanotube (MWCNT). By imaging the MWCNT under different tapping forces, we were able to demonstrate its remarkable reversible radial deformability (up to ~40%) and reveal internal discontinuities along its length. The values of the effective elastic modulus of several sections of the MWCNT in the radial direction were estimated with the Hertz model.

PACS numbers: 62.20.Qp, 61.48.+c, 83.10.Bb

The remarkable mechanical properties of carbon nanotubes (CNTs) have attracted attention both in theoretical and experimental studies. CNTs can have both high modulus and high strength [1–4], which makes them superior to conventional carbon fibers that have only either high modulus or high strength. While the tensile properties of CNTs have attracted the most attention to date, their mechanical response when subjected to load applied in the radial direction has not been thoroughly studied. CNTs are resilient in that they can be elastically bent to large deformation [5–7]. Radial deformation of CNTs has also been observed in several transmission electron microscopy studies [8–11]. Achieving understanding of the radial "deformability" of CNTs is important for applying CNTs as components in future nanomechanical or nanoelectronic systems. For example, radial deformation of CNTs may prominently affect their electrical properties [12–14].

Because of the challenge of applying localized force on such small objects, there has not been any experiment on examining the radial deformability of individual carbon nanotubes. Tapping-mode atomic force microscopy (AFM) has the virtue of allowing the imaging of soft materials and loosely attached small objects because of the virtual elimination of lateral force while preserving high imaging resolution [15]. Here we describe a study on the radial deformability of a multiwalled carbon nanotube (MWCNT) with tapping-mode AFM and show that it is a good tool for studying the deformability of loosely attached objects in the nanometer size range and for revealing what can be present in the internal space of nanotubes.

The MWCNTs used were synthesized by the arc discharge method, purified by oxidation in air, and had diameters ranging from 2–50 nm [16]. A suspension of these MWCNTs in 2-butanone was prepared by sonication. The wafer substrate used in the experiments had a thin thermally grown SiO_2 layer on Si and was patterned by electron beam lithography and plasma etching [17]. The pattern on the surface consisted of 70-nm wide, 17-nm deep parallel trenches spaced 500 nm apart. A drop of the MWCNT suspension was dispersed onto the substrate and dried at room temperature. The sample was examined by AFM (Multi-Mode Scanning Probe Microscope IIIa, Digital Instruments) using a TESP tip (Tapping Mode Etched Silion Probe, Digital Instruments) operated in tapping mode in air. The AFM images were analyzed as captured, without plane fitting.

In tapping-mode AFM imaging, the cantilever is oscillated with amplitude A_0 above the surface. The probe is brought close enough to the sample surface to strike it at the bottom of each oscillation cycle. Such intermittent contacts lead to a decrease of cantilever amplitude to the value A. The surface topography is tracked by rastering the sample with respect to the probe and adjusting its height to maintain constant cantilever oscillation amplitude (constant set point $S = A/A_0$). In the current study, we took advantage of the fact that decreasing the set point leads to an increase of the average force with which the probe strikes the sample [18,19]. We have recently established [20] that for operation in the frequency range $f \leq f_0$, where f_0 is the resonance frequency of a cantilever, the average tapping force F_{av} can be described with a semiempirical formula, derived from computer simulations and validated through direct measurements of the deflection of a soft cantilever under the influence of tapping force:

$$F_{\mathrm{av}} = 0.5k_c(1 - S)A_0(f)/Q\beta\,, \tag{1}$$

where k_c is the force constant of the probe cantilever, Q is its quality factor, and β is the off-resonance parameter defined as

$$\beta = A_0(f)/A_0(f_0)\,, \tag{2}$$

where A_0 denotes the free cantilever amplitude achieved for constant drive amplitude at different frequencies. In this work we used a TESP silicon cantilever with a nominal spring constant $k_c = 50$ N/m and a quality factor (as determined from the width of the resonance peak) $Q = 377$. The cantilever was oscillated with the free amplitude $A_0 = 26$ nm at the frequency corresponding to $\beta = 0.03$.

Figure 1 illustrates the reversible radial deformability of a MWCNT imaged using the approach described above.

 0031-9007/00/85(7)/1456(4)$15.00

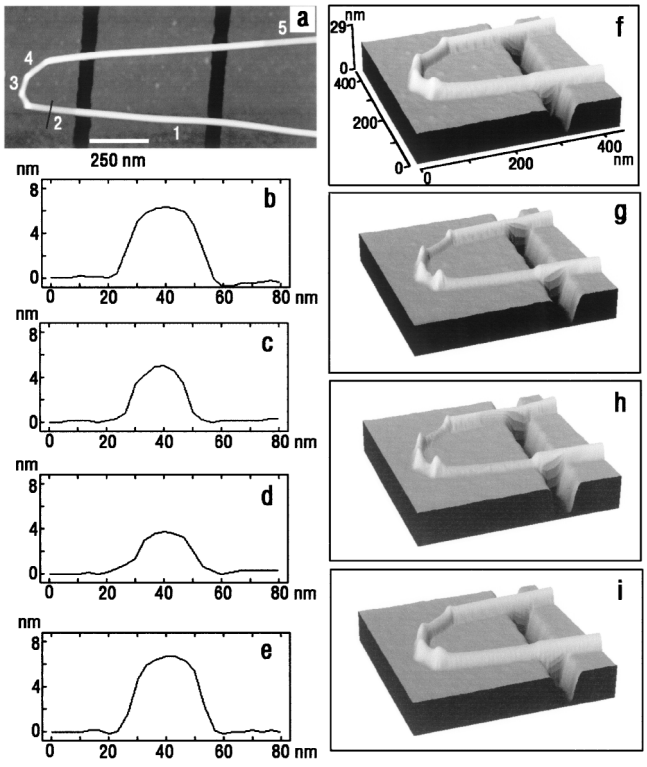

FIG. 1. Deformability of a MWCNT deposited on a patterned silicon wafer as visualized with tapping-mode AFM operated far below mechanical resonance of a cantilever at different set points. The height in this and all subsequent images was coded in gray scale, with darker tones corresponding to lower features. (a) Large-area view of a MWCNT bent upon deposition into a hairpin shape. (b)–(e) Height profiles taken along the thin marked line in (a) from images acquired at different set-point (S/S_0) values: (b) 1.0; (c) 0.7; (d) 0.5; (e) 1.0. (f)–(i) Three-dimensional images of the curved region of the MWCNT acquired at the corresponding set-point values as in (b)–(e).

The MWCNT was bent as a consequence of the deposition into a hairpin shape with four kinks in the curved region [Fig. 1(a)]. Section profiles of the MWCNT taken along the line marked in Fig. 1(a) and shown in Figs. 1(b)–1(e) were obtained with the AFM operated at sequentially decreasing set points ($\sim$1.0, 0.7, 0.5), and then again at $S \sim 1.0$ [Fig. 1(e)]. Corresponding three-dimensional images of the curved region are shown in Figs. 1(f)–1(i). Both height profiles [Figs. 1(b)–1(d)] and three-dimensional images [Figs. 1(f)–1(h)] clearly show the decrease of height of the MWCNT section 2 with the increase of average force (the decrease of set point) from the unperturbed value of $\sim$6.3 nm to the final value of $\sim$3.6 nm, a deformation of 42%. Importantly, this remarkable deformation was reversible [Figs. 1(e) and 1(i)]. In contrast, the depth of the trenches [parallel dark lines in Fig. 1(a)] in the silicon substrate measured from the same images did not change with the changes of the set point, which shows that the AFM operated in this mode was still capable of obtaining real topographical information. The height of the kinks in the MWCNT did not appreciably change with applied force, which is consistent with their expected higher stiffness.

Figure 2(a) shows the results of AFM observations at different set points converted using Eq. (1) into force-strain plots $F_{\mathrm{av}}(\varepsilon)$ in which the strain is defined as

$$\varepsilon = (H_0 - H)/H_0\,, \tag{3}$$

where H_0 and H denote, respectively, the original height and deformed height of a nanotube. The markedly different force-strain plots in Fig. 2(a) correspond to different sections of the nanotube, as indicated and numbered in Fig. 1(a). For sections 2, 3, and 4, the plots initially show a similar linear dependence of deformation of the nanotube on the effective tapping force, while the plots show sections 1 and 5 are significantly more rigid. The observed differences in radial deformability can be explained straightforwardly by the presence of defects such as internal closures and outer layer terminations. Internal closures change the local structure of the MWCNT, so that some sections of the MWCNT have less concentric nested cylinders than others. This makes those sections more deformable when subjected to a concentrated transverse load

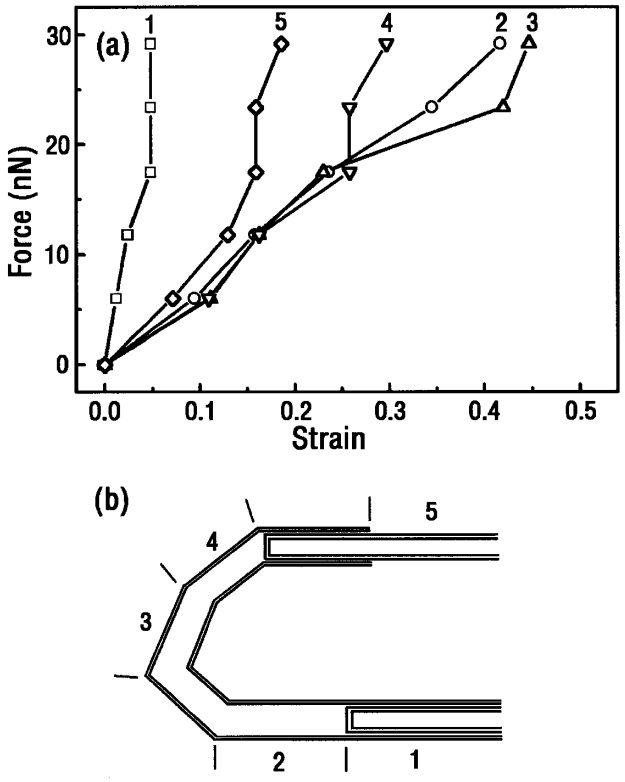

FIG. 2. Radial deformability of the MWCNT. (a) Force-strain curves obtained for different sections of the MWCNT shown in Fig. 1, based on height measurements in images acquired at different set points. Values in parentheses correspond to unperturbed heights of sections, H_0, measured from images acquired at set point close to unity, 1(□, 8.2 nm), 2(○, 6.3 nm), 3(△, 7.3 nm), 4(▽, 7.3 nm), 5(◇, 6.9 nm). (b) A proposed schematic of the structure of MWCNT based on deformabilities of its various sections. Sections are marked according to Fig. 1(a).

than other sections, even if all sections have the same outer diameter. Abrupt termination of the cylinder layer or a step caused by pentagon-heptagon pairs [21] along a MWCNT can lead to a decrease of its outer diameter and to the abrupt change of its stiffness as seen for section 5. The proposed structure of the investigated MWCNT, based on the differences in deformability of its different sections, is shown schematically in Fig. 2(b) (the proposed schematic is only qualitative, since the exact number of layers in each section could not be determined accurately in our experiments). The dependence of radial deformability of nanotube on diameter and the number of nested layers has been predicted by Lordi *et al.*'s simulations [11] of high-speed collision of a C_{60} molecule with a nanotube. The simulation also showed the elastic and reversible character of deformation and the decrease of dependence of stiffness on the number of layers with the increase of nanotube radius. The experimental evidence of radial deformability of MWCNTs was reported in an earlier paper by Ruoff *et al.* [8], who observed a distortion of the cross section and a change of the interlayer spacing in a pair of adjacent nanotubes due to mutual van der Waals attraction. The apparent saturation of the compression observed on sections 1 and 5 is probably related to the compression behavior of graphite, in that a MWCNT with a small inner diameter and a large outer diameter readily reaches the graphite limit, as also mentioned in the paper of Lordi *et al.* [11].

The stiffness of various sections of the MWCNT in the radial direction was determined from the slopes of force-strain curves. It ranged from ~11 N/m (sections 2, 3, and 4) through ~16 N/m (section 5) to ~44 N/m (section 1).

The observed range of stiffness values reflects the structural complexity of the MWCNT. A simple mechanical model is presented below to infer the effective elastic modulus of the MWCNT and is found to be useful for the purpose of making comparison with other materials. In the model, the AFM tip was treated as a uniform sphere of radius R_{tip} and the MWCNT as a uniform, isotropic, and rubberlike solid cylinder characterized by a Poisson ratio $\nu_{\text{NT}} = 0.5$ and an effective elastic modulus E_{NT}. The value of R_{tip} corresponds to the radius of curvature of the AFM tip and can be determined from the apparent width W of the MWCNT from the AFM images, using a simple geometrical "deconvolution" formula $R_{\text{tip}} = W^2/16R_{\text{NT}}$ [22], where R_{NT} denotes the true radius of the MWCNT obtained from the measured height. Based on the height and width measurements of the most rigid section of the nanotube imaged at set points close to unity (minimum tapping force), the tip used in our experiments was characterized by $R_{\text{tip}} = 24$ nm. The AFM tip is made of monocrystalline silicon and has a Young's modulus value of $E_{\text{tip}} = 180$ GPa and a Poisson ratio $\nu_{\text{tip}} = 0.28$. The indentation of a soft cylinder by a rigid sphere can be described using the Hertz model [23]. In this model, the vertical distance z between corresponding points on the sphere surface and the cylinder surface is expressed as

$$z = Ax^2 + By^2, \tag{4}$$

where the z axis is along the line of action of the load and the x-y plane is tangent to both objects at the point of contact. The x axis coincides with the long axis of the cylinder. The shape of the contact area under a load F is assumed to be an ellipse and is described as

$$\frac{x^2}{a^2} + \frac{y^2}{b^2} = 1\,. \tag{5}$$

According to the known solution, the sum of the z direction deformation of two bodies in the contact point $(x, y) = (0, 0)$ can be expressed as [23]

$$\delta = \frac{3FkK(k)\,(A + B)\Delta}{2\pi b}\,, \tag{6}$$

where

$$A = \frac{1}{2R_{\text{tip}}}\,, \qquad B = \frac{1}{2R}\,, \qquad \frac{1}{R} = \frac{1}{R_{\text{tip}}} + \frac{1}{R_{\text{NT}}}$$

and

$$b = \sqrt[3]{\frac{3kF\Delta RE(k)}{2\pi}}\,,$$

where

$$\Delta = \frac{1}{A + B}\left(\frac{1 - \nu_{\text{tip}}^2}{E_{\text{tip}}} + \frac{1 - \nu_{\text{NT}}^2}{E_{\text{NT}}}\right), \qquad k = \frac{b}{a}\,,$$

$$E(k) = \int_0^{\pi/2} \sqrt{1 - (1 - k^2)\sin^2\theta}\, d\theta$$

and k can be determined from the equation

$$\frac{B}{A} = \frac{(1/k^2)E(k) - K(k)}{K(k) - E(k)}\,,$$

where

$$K(k) = \int_0^{\pi/2} \frac{1}{\sqrt{1 - (1 - k^2)\sin^2\theta}}\, d\theta\,.$$

Since the effective elastic modulus E_{NT} of the MWCNT can be expected to be much smaller than that of the silicon AFM tip, the total deflection δ is almost exclusively due to the deformation of the cylinder. Under such circumstances, the "strain" as defined by Eq. (3) is equal to $\varepsilon = \delta/2R_{\text{NT}}$. Equation (6) can then be used to generate the force-strain curves similar to those used to describe the deformability of the MWCNT. As shown in Fig. 3(a), the observed behavior of the MWCNT modeled as a solid cylinder having a diameter of 8 nm could be reproduced using the values of E_{NT} ranging from 0.3 to 4 GPa. These values are comparable with the Young's modulus values of semicrystalline polymers such as *low-density polyethylene* ($E = 0.2$ GPa) or *polyamide 6.6* ($E = 1.9$ GPa) [24]. There is a strong dependence of the mechanical response of the MWCNT on its E_{NT} value, as seen in Fig. 3(a), but a weaker dependence on the diameter of the different sections of the MWCNT, as seen in Fig. 3(b). The observed differences in deformation response are thus primarily due

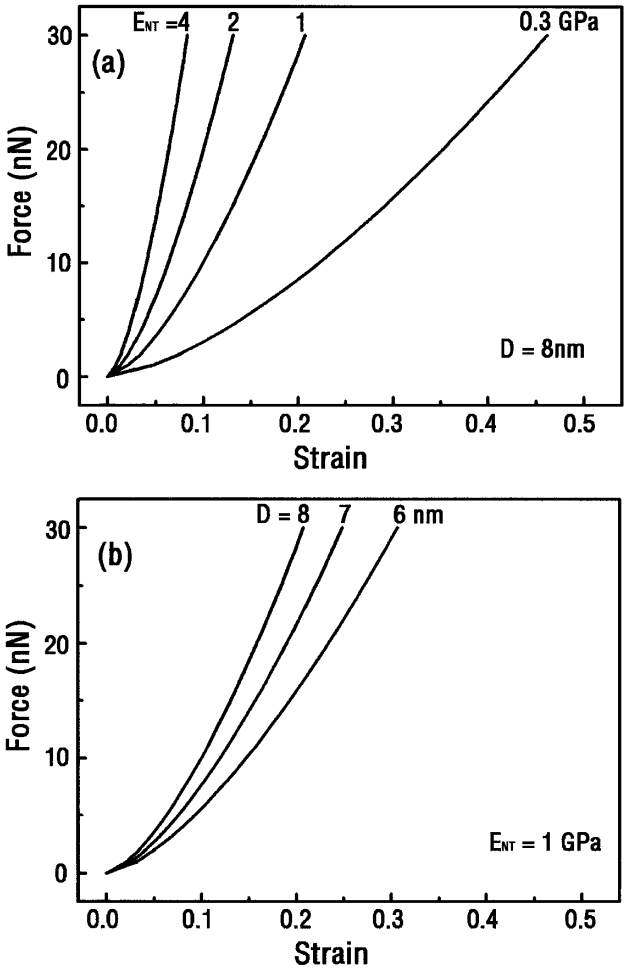

FIG. 3. Force-strain curves calculated from the Hertz model for a system consisting of a soft cylinder indented by a rigid sphere. (a) Results obtained for a cylinder with the diameter of 8 nm and with Young's modulus values chosen to match the observed deformability of MWCNT [Fig. 2(a)]. (b) Force-strain curves calculated for cylinders of different diameters, characterized by Young's modulus of 1 GPa.

to the different stiffness along the MWCNT and not due to the differences in the outer diameter. Note that the elastic constant C_{33} (response to a load in the direction perpendicular to the basal plane) in graphite is 36.5 GPa [21]. The obtained effective elastic modulus values are smaller than C_{33} of graphite because this MWCNT is hollow and has a large diameter.

In summary, a novel approach to tapping-mode AFM, allowing controlled variation and determination of effective tapping force (the load), was used to visualize and measure the reversible transverse deformability of a MWCNT. Internal and external discontinuities along the MWCNT sections were clearly revealed. The estimated values of the effective elastic modulus of the MWCNT in the radial direction are comparable to the Young's modulus values of semicrystalline polymers. The obtained results indicate that although MWCNTs are rigid and strong under tensile load along their axes, owing to their hollow nature they can exhibit significant radial deformability.

We acknowledge partial support for this work by the Office of Naval Research and Defense Advanced Research Programs Agency and by the NSF under the New Tools and Methods for Nanotechnology Grant No. NSF-DMR 9871874. The authors appreciate Brian Faircloth providing the patterned Si sample and W. Chen for useful discussions.

*Electronic address: tomek@wuchem.wustl.edu
Address after 1 September 2000: Department of Chemistry, Carnegie Mellon University, Mellon Institute, 4400 Fifth Avenue, Pittsburgh, PA 15213-2683. (tomek@andrew.cmu.edu)
†Electronic address: ruoff@wuphys.wustl.edu
Address after 1 September 2000: Department of Mechanical Engineering, Northwestern University, 2145 Sheraton Road, Evanston, IL 60208-3111. (r-ruoff@northwestern.edu)

[1] A. Krishnan *et al.,* Phys. Rev. B **58**, 14 031 (1998).
[2] P. Poncharal *et al.,* Science **283**, 1513 (1999).
[3] J.-P. Salvetat *et al.,* Phys. Rev. Lett. **82**, 944 (1999).
[4] M.-F. Yu *et al.,* Science **287**, 637 (2000).
[5] M. R. Falvo *et al.,* Nature (London) **389**, 582 (1997).
[6] B. I. Yakobson, in *Proceedings of the Symposium on Fullerenes, Electrochemical Society,* edited by R. S. Ruoff and K. M. Kadish (ECS, Pennington, 1997), p. 549.
[7] M. Buongiorno Nardelli, B. I. Yakobson, and J. Bernholc, Phys. Rev. B **57**, R4277 (1998).
[8] R. S. Ruoff *et al.,* Nature (London) **364**, 514 (1993).
[9] J. Tersoff and R. S. Ruoff, Phys. Rev. Lett. **73**, 676 (1994).
[10] N. G. Chopra *et al.,* Nature (London) **377**, 135 (1995).
[11] V. Lordi and N. Yao, J. Chem. Phys. **109**, 2509 (1998).
[12] R. Martel *et al.,* Appl. Phys. Lett. **73**, 2447 (1998).
[13] C.-J. Park, Y.-H. Kim, and K. J. Chang, Phys. Rev. B **60**, 10 656 (1999).
[14] P. E. Lammert, P. Zhang, and V. H. Crespi, Phys. Rev. Lett. **84**, 2453 (2000).
[15] Q. Zhong *et al.,* Surf. Sci. Lett. **290**, L688 (1993).
[16] J. H. Hafner, Nanotube tips for AFM, at http://www.cnst.rice.edu/mount.html on the Internet. We appreciate receiving this sample from the Smalley group at Rice University.
[17] We acknowledge the use of the Cornell Nanofabrication Facility where electron beam lithography and plasma etching were used to pattern trenches.
[18] R. Garcia and A. S. Paulo, Phys. Rev. B **60**, 4961 (1999).
[19] S. C. Fain, Jr. *et al.,* Appl. Phys. Lett. **76**, 930 (2000).
[20] T. Kowalewski (to be published).
[21] T. W. Ebbesen, *Carbon Nanotubes: Preparation and Properties* (CPC Press, New York, 1997).
[22] C. T. Gibson, G. S. Watson, and S. Myhra, Scanning **19**, 564 (1997).
[23] A. P. Boresi and O. M. Sidebottom, *Advanced Mechanics of Materials* (John Wiley & Sons, New York, 1985).
[24] H. G. Elias, *An Introduction to Polymer Science* (VCN Publishers, New York, 1997).